ACS OMEGA

http://pubs.acs.org/journal/acsodf

Article

A Co(III) Complex of 1-Amino-4-hydroxy-9,10-anthraquinone Exhibits Apoptotic Action against MCF-7 Human Breast Cancer Cells

Somenath Banerjee, Sanjay Roy, Dhanasekaran Dharumadurai, Balaji Perumalsamy, Ramasamy Thirumurugan, Saurabh Das,* Asoke Prasun Chattopadhyay,* and Partha Sarathi Guin*

Cite This: *ACS Omega* 2022, 7, 1428−1436

Read Online

ACCESS | Metrics & More | Article Recommendations | Supporting Information

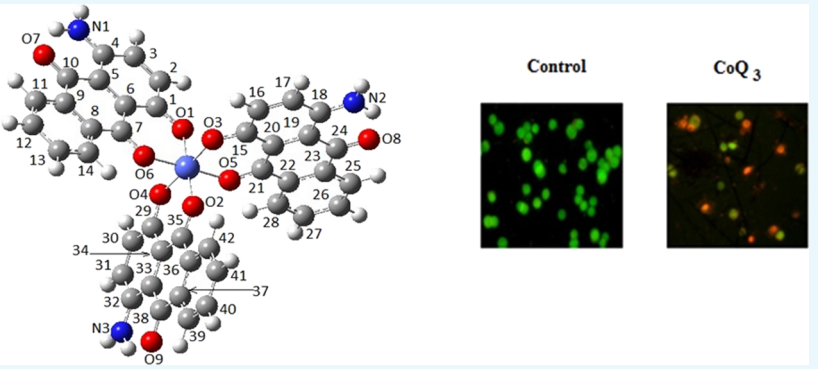

ABSTRACT: A Co(III) complex of 1-amino-4-hydroxy-9,10-anthraquinone (QH) (Scheme-1) having the molecular formula CoQ_3 (Scheme-2) was prepared and characterized by elemental analysis, FTIR spectroscopy, UV−vis spectroscopy, fluorescence spectroscopy, and mass spectrometry. In the absence of a single crystal, the energy-optimized molecular structure of CoQ_3 was determined by employing computational methods that was validated using spectroscopic evidences, elemental analysis, and mass spectrometry data. The electrochemical properties of the complex were analyzed using cyclic voltammetry and indicate a substantial modification of the electrochemical properties of the parent amino-hydroxy-9,10-anthraquinone. CoQ_3 was thereafter tested on MCF-7 human breast cancer cells. The IC_{50} value for a 24 h incubation was found to be (95 ± 0.05) μg/mL. The study showed that such cancer cells underwent both early and late apoptosis following the interaction with CoQ_3.

1. INTRODUCTION

Anthracycline drugs are anticancer agents used in treating different forms of human carcinoma.[1−4] Although they enjoy wide acceptance in chemotherapy, their use is often questioned for the associated cardiotoxicity and high cost involved, particularly for people from economically weaker sections of the society. Hence, there is an effort worldwide[5−19] to find alternative cheaper analogues that are less cardiotoxic.[5−10] These are either derivatives of anthracyclines that are less costly or their simpler analogues.[11−20]

The limitation due to acute and chronic toxicity,[21−25] of which cardiotoxicity receives the maximum attention, is the most disturbing regarding the use of anthracyclines or their derivatives and analogues as anticancer agents.[26−31] Participating in reactions of the respiratory chain, they produce semiquinone radical anions and related intermediates by one-electron reduction of the quinone. Although a pre-requisite for chemotherapeutic efficacy, such generation is also responsible for cardiotoxicity.[26−30] Semiquinone upon reaction with O_2 generates superoxide radical anion ($O_2^{\bullet-}$) that in turn produce H_2O_2/$OH^{\bullet}$.[20,30−33] These species participate in a wide range of redox reactions as in oxidative phosphorylation, complex formation with phospholipid, and in lipid peroxidation.[30−32]

Previous research on the subject suggests that complex formation of these drugs with different metal ions leads to decreased toxicity, the magnitude of which depends on the metal ion. Those metal ions having a stable lower oxidation state were found to cause maximum decrease in $O_2^{\bullet-}$formation in an assay where NADH was the electron donor and cytochrome c was the electron acceptor. Hence, studies related to metal complexes gained a lot of importance regarding this matter.[7,12,14,31,32] Metal complexes stabilize the semiquinone radical anion formed. Hence, superoxide formation due to a reaction between a semiquinone radical anion and molecular oxygen is either inhibited or decreased drastically. It is

Received: November 1, 2021
Accepted: December 22, 2021
Published: December 29, 2021

https://doi.org/10.1021/acsomega.1c06125
ACS Omega 2022, 7, 1428−1436

therefore imperative to study such metal complexes, particularly with regard to their electrochemical behavior under different experimental conditions.

It is worth mentioning that although several metal complexes of adriamycin, daunorubicin, mitoxantrone, and their analogues with Fe(III), Al(III), Cu(II), Ni(II), Pd(II), and Tb(III) were prepared and characterized,[7,10−14,33−46] comprehensive knowledge on structures of these metal complexes is lacking due to inherent difficulties in obtaining single crystals for X-ray diffraction studies. Single-crystal X-ray diffraction structures of only a few hydroxy-9,10-anthraquinone complexes are reported.[44,47,48] In this study also, different methods were employed to obtain single crystals of CoQ_3 taking different compositions of solvents. However, all efforts in getting an appropriate single crystal for CoQ_3 failed. The planarity of the anthraquinone unit in these complexes could possibly be a hindrance in getting single crystals.[7] For this reason, we made an effort to characterize CoQ_3 theoretically using density functional theory (DFT) based on experimental data we obtained such as elemental analysis, IR spectroscopy, mass spectrometry, powder X-ray diffraction, molecular spectroscopy, and electrochemistry. DFT is helpful in generating the energy optimized structure, and various essential parameters of the complex may also be obtained from this study. The thus prepared complex was tested on MCF-7 human breast cancer cells to see whether it initiates apoptosis and thus could be considered as a less costly alternative to anthracyclines already in use.

Scheme 1. 1-Amino-4-hydroxy-9,10-anthraquinone (QH)

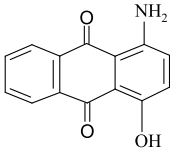

2. RESULTS AND DISCUSSION

2.1. Analysis of the Mass Spectra of CoQ_3. Assuming that the formula of the complex is CoQ_3 (Scheme 2), an analysis of its mass spectrum (Figure S1, SI) was attempted. The molecular ion peak or that of the protonated molecular ion expected at m/z = 773.62 was not found. However, a clear signal at m/z = 689.46 corresponds to a fragment remaining of the complex following loss of a carbon-bound $-NH_2$ group from each ligand (a loss of 28 mass units from each ligand, i.e., 78 mass units from the complex) to result in a peak theoretically expected at m/z = 689.62. From this peak, loss of two quinone oxygens would result in a peak theoretically expected at m/z = 661.62. The experimental value is 661.45, which tallies with the expected value. Loss of four quinone oxygens from the first fragment results in a peak theoretically expected at m/z = 633.62 and experimentally found at 633.42. Here also, the agreement is close. Similarly, loss of six quinone oxygens from all the three ligands of the first fragment should result in a theoretical peak at m/z = 605.62. This was experimentally observed at 605.39, again pointing to a close agreement. At this stage of fragment formation in mass analysis, the metal center is bound to three ligands via the three phenolic −OH groups on each of them. The peaks identified above therefore categorically indicate the formation of a 1:3 complex. Subsequent to the fragmentations mentioned above, further loss of two carbon atoms and a few hydrogens at a time explains peaks at an m/z value of 577.35 and also the cluster of peaks at m/z values of 533.99, 532.99, and 531.98, respectively. Peaks at lower m/z values correspond to smaller fragments. Therefore, from an analysis of the mass spectrum of the cobalt complex, it may be concluded that the complex has the formula CoQ_3 as shown in Scheme 2.

Scheme 2. Structure of CoQ_3

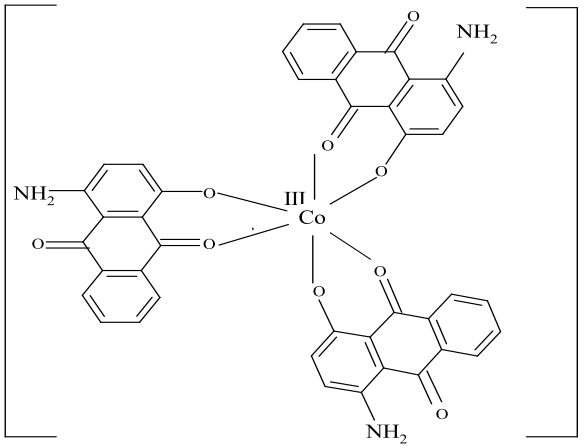

2.2. Analysis of the IR Spectra of CoQ_3. The FTIR spectrum for QH (Figure S2, SI) shows a peak at 3431 cm^{-1}, which is due to N−H bond stretching, while that at 3300 cm^{-1} is due to stretching of O−H bonds.[6] The O−H stretching is modified significantly in the complex (Figure S3, SI), indicating an involvement of the −OH group during complex formation. Since there is deprotonation of −OH during complex formation, the molecule ceases to show intramolecular hydrogen bonding identified in QH. Peaks in this region do not disappear completely in the complex when compared with QH, indicating the presence of free $-NH_2$ on each ligand (just as that observed or the IR spectrum of QH). In the IR spectrum of CoQ_3 (Figure S3, SI), peaks at 1625, 1586, and 1537 cm^{-1} are attributed to stretching due to free carbonyl and C=C or a combination of both, respectively. In an earlier study,[6] we showed that peaks obtained in the region 1464−1031 cm^{-1} in the IR spectrum of the ligand (QH) may be attributed to combinations of O−H, N−H, and C−H bending modes. Natures of the peaks in this region are somewhat different in the complex. More specifically, the peak at 1121 cm^{-1} is reduced significantly, probably due to binding of oxygen of the −OH group to Co(III) following its deprotonation.

2.3. Powder X-ray Diffraction of CoQ_3. The powder X-ray diffraction (PXRD) pattern of CoQ_3 is shown in Figure 1. All peaks can be indexed with the space group $R32(155)$, and Cu Kα = 1.5406 Å using the WINPLOTR program. Refined cell parameters were found to be a = 7.45 Å, b = 6.52 Å, and c = 27.8 Å. The unit cell volume was 1352 $Å^3$; α = 33.43°, β = 90°, and γ = 90°. Thus, PXRD analysis provides information about the dimension of the unit cell of a crystalline CoQ_3.

2.4. Structure of $CoQ_3$from Density Functional Theory Methods. The energy-optimized molecular structure of CoQ_3 is shown in Figure 2, and structural parameters are summarized in Table S1 (SI). Figure 2 shows three QH molecules coordinated to Co(III) through phenolic O^- and quinone oxygen, forming CoQ_3.

https://doi.org/10.1021/acsomega.1c06125
ACS Omega 2022, 7, 1428−1436

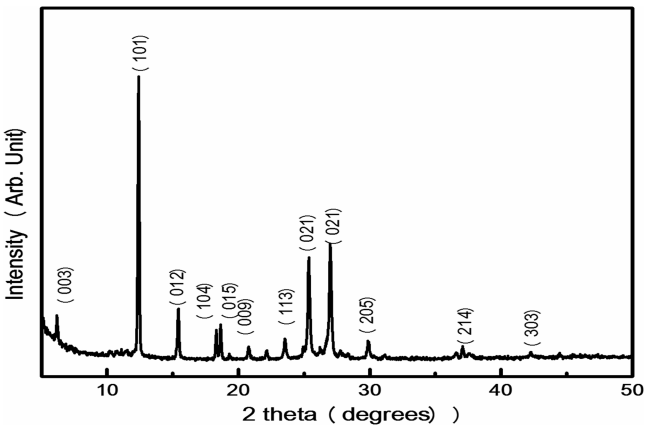

Figure 1. Powder X-ray diffraction patterns of CoQ_3.

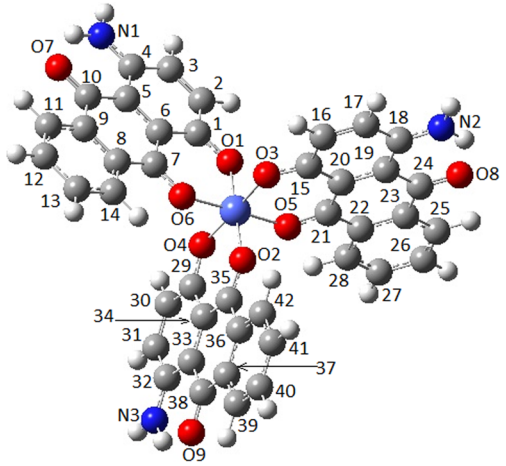

Figure 2. Energy optimized structure of CoQ_3.

The energy level diagrams of QH and CoQ_3 are shown in Figure S3 (SI). The HOMO (H) and LUMO (L) are indicated in each case (Figure 3). Red lines indicate the π

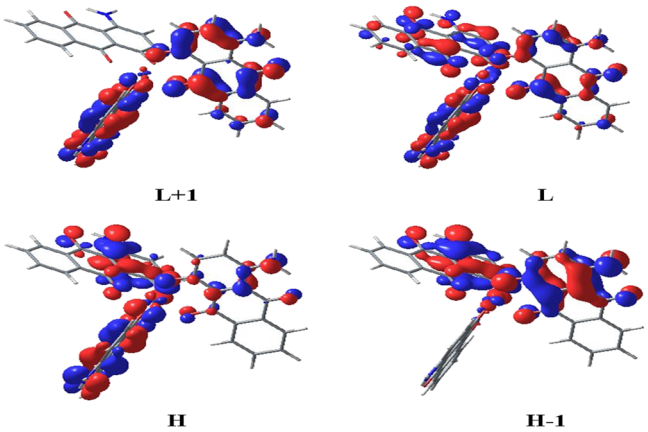

Figure 3. Different HOMOs (H) and LUMOs (L) of CoQ_3.

orbitals, black lines indicate σ, and blue lines represent mixed metal−ligand (M-L) orbitals. Some M-L type MOs may have mixed σ and π characters as the three ligands are arranged in such a manner that σ of one may mix with π of another. Metal orbitals are mainly dπ, with some pπ mixed. Co(III) orbitals are much lower in energy to be shown in the above diagram. It should also be noted that the HOMO and LUMO are M-L type orbitals.

2.5. UV−vis Spectroscopy of CoQ_3. The absorption spectrum of QH (Figure 4a) in 30% ethanol[6,7] shows four absorption bands (at 250, 290, 530, and 565 nm) due to $\pi-\pi^*$ and n$-\pi^*$ transitions of its various tautomeric forms in rapid equilibrium in aqueous solution.[6,7,49] From the UV−vis spectrum of CoQ_3 (Figure 4b), it is clear that the absorption peaks at 250, 290, 530, and 565 nm remain almost unaltered, which indicate that the electronic absorption spectrum of CoQ_3 depends weakly on the nature of the metal and is primarily defined by the ligand (QH).[49] However, the appearance of a new peak at 600 nm is characteristic of the complex (CoQ_3). It is important to mention here that tautomeric structures found for free QH[49] in aqueous media are not possible for CoQ_3 since phenolic −OH groups in the QH molecule are deprotonated owing to coordination of Co(III) by phenolic oxygens.

2.6. Fluorescence Spectroscopy of CoQ_3. Fluorescence spectra of QH and CoQ_3 are shown in Figure S4 (SI) recorded following an excitation at 530 nm. The emission spectrum exhibits a maximum at 590 nm for QH and 594 nm for CoQ_3. The difference in the emission peak of CoQ_3 compared to QH is due to the metal ligand bond.

2.7. Electrochemical Reduction of CoQ_3 in Organic Polar Solvents. Electrochemical behavior of CoQ_3 was studied in anhydrous DMSO and DMF in the presence of TBAB as the supporting electrolyte using cyclic voltammetry. In anhydrous DMSO, CoQ_3 undergoes successive three one-electron reductions having peak potentials (E_{pc}) at −0.795, −1.010, and − 1.295 V, respectively, vs Ag/AgCl/saturated KCl (Figure 5 and Table 1). In this case, the first reduction is reversible, while the other two are quasi-reversible at different scan rates. These three one-electron reduction steps are due to the reduction of the three free quinone centers of the three Q^- bound to Co(III) inCoQ_3 (Scheme 3). For these reductions, the formal potentials (E) of the respective reduction steps were found at −0.750, −0.987, and −1.255 V, respectively. It is noted that although there are three equivalent free quinone sites in CoQ_3 (Scheme 3), there exists a difference in their formal potential values, which is quite appreciable. Thus, after reduction at the first free quinone in CoQ_3, reduction of the second and third quinone sites is significantly delayed. In other words, the reduced species (semiquinone radical anion) that formed due to the first or second reduction is stabilized in the metal ion environment due to delocalization of the negative charge. This is important with regard to the compound's biochemical action since a stabilized semiquinone would delay the reaction between semiquinone and molecular oxygen[30−34] within cells where it would be employed.

In anhydrous DMF, under similar experimental conditions, CoQ_3 undergoes three-one electron reductions having peak potentials (E_{pc}) at −1.025, −1.225, and −1.475 V, respectively, with the corresponding formal potentials (E) being −0.950, −1.195, and −1.405 V, respectively (Figure 6 and Table 1). Considering the fact that the polarity of DMF is less than that of DMSO[51] and comparing the three reduction potentials of CoQ_3 in the two solvents, it can be said that with the increasing polarity of the medium, reduction potentials move in a positive direction and that reductions become more feasible as the polarity of solvent increases. This means stability of the formed semiquinone species is increased with an increase in the polarity of the medium. Stabilization of the

https://doi.org/10.1021/acsomega.1c06125
ACS Omega 2022, 7, 1428−1436

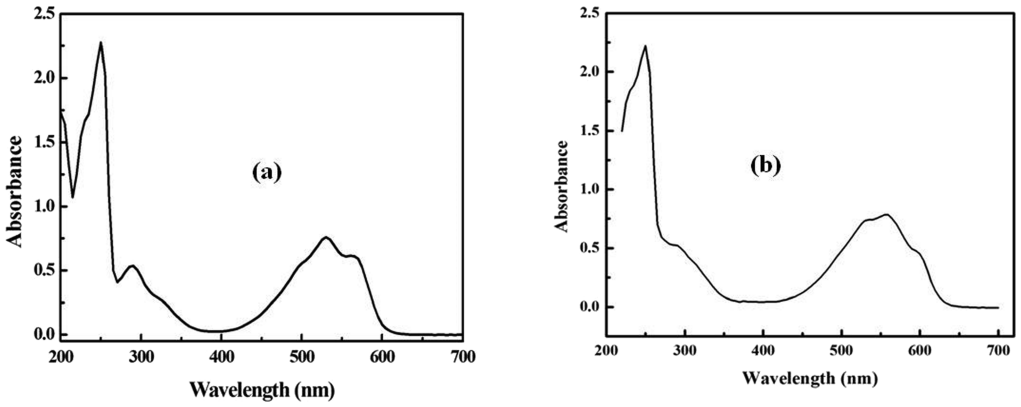

Figure 4. UV−vis spectrum of (a) QH and (b) CoQ_3 in aqueous ethanol.

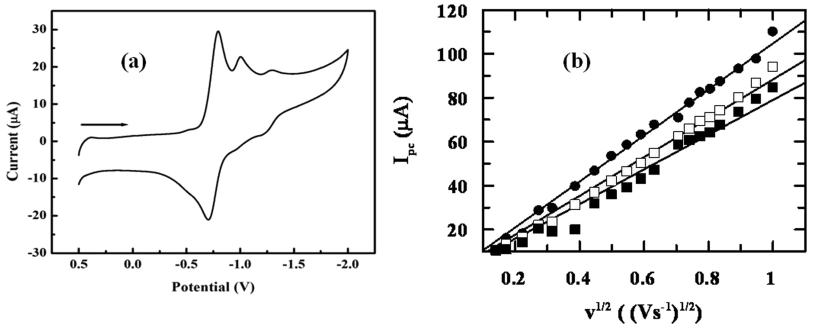

Figure 5. (a) Cyclic voltammogram of CoQ_3 in anhydrous DMSO media. Scan rate: 0.10 Vs^{-1}. [CoQ_3] = 1 × 10^{-3} M, [TBAB] = 0.1 M, T = 298.15 K. (b) Plot of cathodic peak current vs square root of scan rate for first (solid circles), second (open squares), and third reduction (solid squares) of CoQ_3 in anhydrous DMSO.

Table 1. Electrochemical Parameters of CoQ_3[a]

media	Epc-1 (V)	Epc-2 (V)	Epc-3 (V)	E-1 (V)	E-2 (V)	E-3 (V)	D_0 (cm^2 s^{-1})
DMSO	−0.795	−1.010	−1.295	−0.750	−0.987	−1.255	3.04 × 10^{-5}
DMF	−1.025	−1.225	−1.475	−0.950	−1.195	−1.405	6.31 × 10^{-5}

[a]Potentials were measured with respect to vs Ag/AgCl/saturated KCl.

semiquinone is also reflected in the formal reduction potential data. This aspect is important with respect to its chemotherapeutic efficiency.[30−34] Owing to stabilization of the semiquinone radical anion, the probability for reaction of a semiquinone radical anion with molecular oxygen would be delayed and that may reduce cardiotoxicity if the molecule were to be employed as an anticancer agent.[30−34]

Under similar experimental conditions, a cyclic voltammogram of QH shows two reversible waves at −0.816 and −1.355 V in anhydrous DMSO and at −0.832 and −1.309 V in anhydrous DMF vs Ag/AgCl, with saturated KCl forming a semiquinone radical anion and quinone dianion, respectively.[7,8] Formal potentials for such reductions were evaluated as −0.770 and −1.308 V in anhydrous DMSO and −0.785 and −1.258 V in anhydrous DMF.[8] Comparing electrochemical parameters and cyclic voltammograms (Figures 5 and 6) of CoQ_3 with those of QH in anhydrous DMSO and anhydrous DMF,[8] one can say that the electrochemical behavior of QH bound to a metal ion as Q^-(as in CoQ_3) is significantly altered.

It is seen that the reduction peak currents (I_{pc}) for three successive reductions of CoQ_3 in both DMSO and DMF have a linear relationship with the square root of the scan rate and that it passes through the origin (Figures 5 and 6). This suggests that such reductions are fully diffusion controlled and that there is no adsorption on the electrode surface. The diffusion coefficient (D_O) of CoQ_3 was determined by the relation shown in eq 1[50] and found as 3.04 × 10^{-5} and 6.31 × 10^{-5} cm^{2}s^{-1} in DMSO and DMF, respectively (summarized in Table 1).

$$I_{pc} = (2.69 \times 10^5) n^{3/2} D_O^{1/2} A C v^{1/2} \quad (1)$$

where I_{pc} = cathodic peak current (A), n = number of electron involved in the reduction, A = area of the electrode (cm^2), C = concentration (mol·cm^{-3}), and v = scan rate (V·s^{-1}).

From values of diffusion coefficients of CoQ_3 in two different solvents (Table 1), it is evident that D_O increases as the polarity of the solvent decreases, clearly indicating greater solvation of CoQ_3 in a more polar solvent that causes lower diffusion onto the surface of the electrode. Thus, CoQ_3 is more solvated in DMSO due to hydrogen bonding and other electrostatic interactions.[8] Intermolecular hydrogen bonding between one of the two hydrogen of aromatic amino group (−NH_2) of QH and negatively charged oxygen of the solvent (DMSO) is very strong.[8] This type of hydrogen bonding would be weak in the case of DMF since for this solvent, oxygen has a less partial negative charge than that on oxygen in DMSO.[8]

https://doi.org/10.1021/acsomega.1c06125
ACS Omega 2022, 7, 1428−1436

Scheme 3. Three Step One-Electron Reductions of CoQ_3 in Organic Polar Solvents Like DMSO and DMF

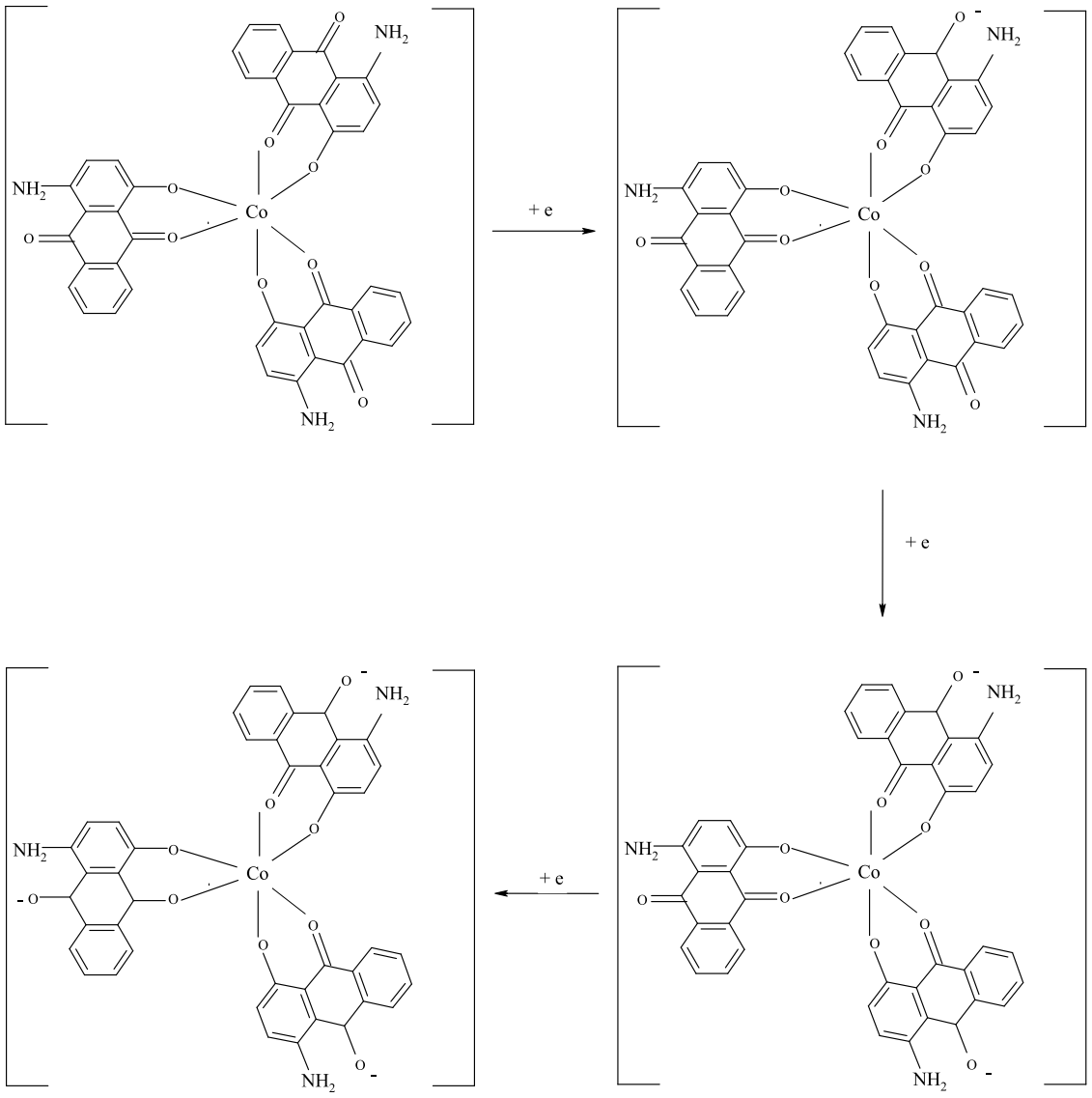

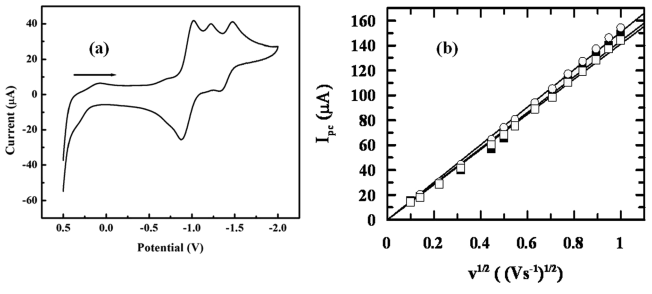

Figure 6. (a) Cyclic voltammogram of CoQ_3 in anhydrous DMF media. Scan rate: 0.10 Vs^{-1}. $[CoQ_3] = 1 \times 10^{-3}$ M, [TBAB] = 0.1 M, T = 298.15 K. (b) Plot of cathodic peak current vs square root of scan rate for first (open circles), second (open squares), and third reduction (solid squares) of CoQ_3 in anhydrous DMF.

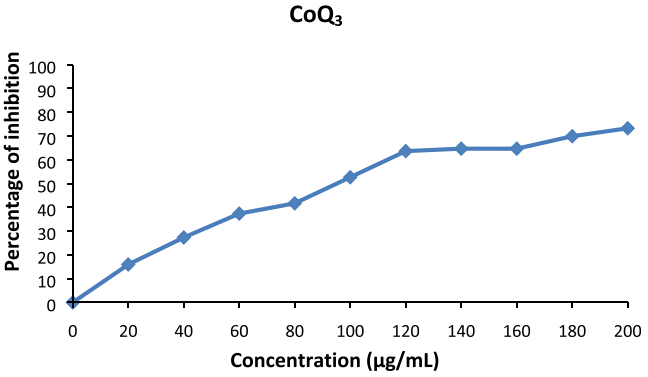

Figure 7. Cytotoxic effect of CoQ_3 on MCF-7 human breast cancer cells after exposure for 24 h.

2.8. Effect of CoQ_3 on Viability of MCF-7 Human Breast Cancer Cells by the MTT Assay. Using the MTT assay, the cytotoxic activity of CoQ_3 was analyzed against MCF-7 human breast cancer cells (Figure 7). It was estimated according to dose values of exposure of CoQ_3 required to reduce the survival to 50% (IC_{50}) in comparison to that of untreated cells. The IC_{50} value for 24 h was found to be (95 ± 0.05) μg/mL. This indicates that CoQ_3 is cytotoxic against MCF-7 breast cancer cells.

2.9. AO/EB Staining. Apoptosis is the hallmark of cell death and can be characterized by cellular morphological

https://doi.org/10.1021/acsomega.1c06125
ACS Omega 2022, 7, 1428−1436

changes observed during the process of cell death. The dual staining method of AO/EB detects such morphological changes. Figure 8 corresponds to AO/EB staining of

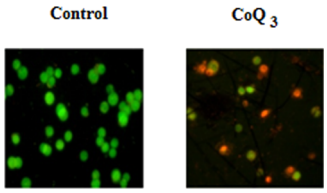

Figure 8. AO/EB staining of the control and CoQ_3-treated MCF-7 human breast cancer cells.

control/non-treated and CoQ_3-treated MCF7 breast cancer cells. Based on fluorescence emission and nucleus morphology, cells were distinguished to have viable, apoptotic, or necrotic characteristics. The viable cells were observed to have uniform green-colored nuclei with a typical cell morphology and intact membrane. On the other hand, apoptotic cells showed irregular cell morphologies with orange to red condensed chromatin and/or fragmented nuclei. Furthermore, the large orange to red fluorescent swollen cells with no fragmented nuclei were differentiated as necrotic cells. The results from AO/EB staining reveal that the control group contains more viable cells and a few apoptotic and necrotic cells. In contrast, CoQ_3-treated MCF7 breast cancer cells induced majority of cell death through the apoptosis mode and actually very few by necrosis. Furthermore, condensed and fragmented morphologies were mostly observed in the CoQ_3 treatment group. The results of calculating the percentage of apoptotic cell death induced by CoQ_3 and analyzed by fluorescent images of AO/EB staining revealed that AQS-treated cells induced a higher percentage of apoptotic cells and a lower percentage of necrotic cells than untreated cells (Figure 9). The graph depicts a percentage count of apoptotic normal and abnormal cells. The error bar represents the standard deviation across three replicates.

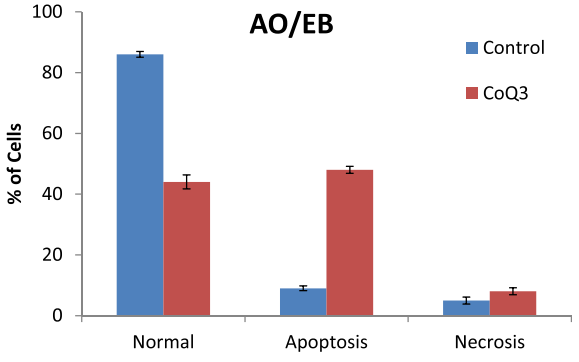

Figure 9. Comparison of percentage of cells in apoptotic death compared to healthy cells and necrotic death.

3. CONCLUSIONS

A Co(III) complex of 1-amino-4-hydroxy-9,10-anthraquinone (QH) with the molecular formula CoQ_3 was synthesized and characterized by different methods. The optimized molecular structure of CoQ_3 was estimated using computational methods. The HOMO and LUMO of CoQ_3 were also characterized by this method. Electrochemical properties of CoQ_3 were studied in anhydrous DMSO and anhydrous DMF media using cyclic voltammetry, and the mechanism of reduction was established. It showed that different reduced anions of CoQ_3 are stabilized in a metal surrounding environment and that reductions would therefore be delayed. Polarity of the solvents also affects stability of the reduced anion. A significant modification of electrochemical properties of QH was also seen when it was bound to Co(III) in CoQ_3. The IC_{50} value of CoQ_3 for 24 h of incubation corresponding to cytotoxicity of CoQ_3 on human breast cancer cells MCF-7 was evaluated as 95 ± 0.05 μg/mL. The study revealed that such cancer cells underwent both early and late apoptosis due to CoQ_3.

4. EXPERIMENTAL SECTION

4.1. Materials. 1-Amino-4-hydroxy-9, 10-anthraquinone (QH) (Scheme 1) (96%) purchased from Alfa Aesar, Germany was recrystallized from an ethanol−methanol mixture and characterized as mentioned earlier.[6−9] The quinone moiety being sensitive to light, solutions were prepared either just before an experiment or very carefully stored in the dark. $CoCl_2{\cdot}6H_2O$ purchased from Merck, India was used to prepare the Co(III) complex. KCl and tetrabutyl ammonium bromide [TBAB] (both are AR grade, Spectrochem, India) were used as supporting electrolytes in aqueous and non-aqueous media, respectively.

Dimethyl sulfoxide (DMSO) (99.0%, Spectrochem, India) was first dried over fused $CaCl_2$ for 3−4 days, decanted, and then distilled under reduced pressure.[51] The distilled sample was preserved in a well-stoppered Jena bottle in desiccators and redistilled again before use. *N*,*N*-Dimethyl formamide (DMF) (99.5%, Spectrochem, India) (LR, BDH) was purified[52] first by distilling under reduced pressure in a N_2 atmosphere and then preserving the distillate over dry K_2CO_3 (Merck) for a week. Then, the DMF was decanted and allowed to mix with dry P_2O_5 (Riedel) and distilled again to be able to use it under anhydrous conditions. Anhydrous DMF and DMSO were used as solvents in electrochemistry experiments. All aqueous solutions were prepared in triple-distilled water.

4.2. Synthesis of CoQ_3. An aqueous solution of 0.5 mmol $CoCl_2{\cdot}6H_2O$ and a solution of 1.5 mmol QH in acetonitrile were mixed and stirred for about 6 h using a magnetic stirrer. Co(II) was oxidized to Co(III) by purging air into the reaction media. The solution was kept for 7 days in air to allow it to evaporate till it was almost 5 mL. A violet-colored complex was separated by filtration followed by washing with acetonitrile. The complex was recrystallized from a methanol−acetonitrile mixture and dried in air. Results of elemental analysis showed that it has the formula CoQ_3. Found: C, 65.09%; H, 3.08%; N, 5.51%. Calculated: C, 65.13%; H, 3.10%; N, 5.43%. In 25% aqueous ethanol solution, 0.1 mM CoQ_3 showed a conductance less than 5 μS/cm at 298.15 K, indicating that it is neutral.

4.3. Computational Studies. The structure of CoQ_3 was optimized using DFT with Ahlrich SV basis[53,54] and B3LYP functional[55−57] using the Orca program suite.[58] Electronic transitions were calculated by the time-dependent DFT method with the same basis set and functional using Orca. Pictures of molecular orbitals (MOs) were generated with the same basis set and functional using Gaussian 09W[59] and MaSK software.[60]

4.4. Analytical Methods. With the help of a Perkin-Elmer 2400 II elemental analyzer, the carbon, hydrogen, and nitrogen

https://doi.org/10.1021/acsomega.1c06125
ACS Omega 2022, 7, 1428−1436

analyses were done. FTIR analysis was performed on a Perkin Elmer RX-I spectrophotometer. Spectra were obtained using KBr pellets in the range 4000−400 cm^{-1}. The mass spectrum was recorded on Micromass Q-Tofmicro, Waters Corporation. CoQ_3 was dissolved in an anhydrous acetonitrile solvent, and the MS data were recorded by using ESI positive mode. The instrument applies a focusing voltage to the electrospray probe to promote mobile phase evaporation as part of the ionization process. PXRD data was collected on a Bruker AXS D8 powder diffractometer using Cu Kα radiation (λ = 1.548 Å) generated at 40 kV and 40 mA. UV−visible spectroscopy was done on a spectrophotometer (model: MECASYS OPTIZEN POP). Experiments related to cyclic voltammetry were performed using the conventional three-electrode system. The temperature was maintained at 25 °C with the help of a circulating water bath. The working electrode was glassy carbon, the surface area of which was 0.07065 cm^2, the counter electrode was a platinum wire, and the reference electrode was Ag/AgCl in satd. KCl. Using a potentiostat (model DY2312, Digi-Ivy), all electrochemical studies were performed. The range of concentrations of different solutions was 5×10^{-5} $moldm^{-3}$ to 1.5×10^{-3} $moldm^{-3}$. Before the solutions were subjected to cyclic voltammetry, they were degassed for nearly30 min using highly pure Ar.

4.5. Cell Culture. MCF7 human breast cancer cells were procured from National Center for Cell Science, Pune, India. Cells were cultured and maintained in DMEM high-glucose medium (Sigma-Aldrich, USA) supplemented by 10% fetal bovine serum (Gibco, Thermo Fisher, USA) and 20 mL of penicillin/streptomycin as antibiotics (Gibco, Thermo Fisher, USA), and incubated at 37° C with 5% CO_2 in a CO_2 incubator (Thermo scientific, USA). All experiments were carried out using cells from the passage of 15 or less.

4.6. Cell Viability Assay. CoQ_3 was dissolved in DMSO and a stock solution was prepared. It was then diluted to obtain different concentrations of the compound in the range 0−200 μg/mL. Two hundred microliters of such solutions was added to wells containing 5×10^3 MCF-7 cells per well of a 96-well culture plate. DMSO was used as the control solvent. Twenty microliters of MTT solution (5 mg/mL in PBS) was transferred to each well following 24 h of incubation, and the plate was incubated at 37 °C for 4 h in the dark. To dissolve formazan crystals, 100 μL of DMSO was added to each well and the absorbance of the final solution was measured at 570 nm using a microplate reader (Bio-Rad, iMark, USA). Data was collected for three replicates each, and the respective mean was used in the following formula to calculate percentage inhibition:

percentage inhibition = ([mean OD of untreated cells (control) − mean OD of treated cells (treated)] × 100)/(mean OD of untreated cells (control))

4.7. Acridine Orange (AO) and Ethidium Bromide (EB) Staining. CoQ_3-induced apoptosis was examined using the fluorescent-based dual staining method AO/EB as defined by Spector et al.[61] with some modifications. In brief, cells treated for 24 h with the IC_{50} concentration of CoQ_3 were harvested and washed with cold PBS. Cell pellets were resuspended and diluted with PBS. The cell suspension (5000 in number) was mixed with AO/EB solution (3.8 μM AO and 2.5 μM EB in PBS) and transferred to a clean microscope slide. Morphological features of the cells were examined under a fluorescent microscope (Carl Zeiss, Axioscope2plus) with a UV filter (450−490 nm).

■ ASSOCIATED CONTENT

Supporting Information

The Supporting Information is available free of charge at https://pubs.acs.org/doi/10.1021/acsomega.1c06125.

(Figure S1) Mass Spectrum of CoQ_3, (Figure S2) IR spectrum of QH and CoQ_3, (Figure S3) energy level diagram of QH and CoQ_3, (Figure S4) fluorescence spectra of QH and CoQ_3 in aqueous ethanol, and (Table S1) structural parameters of CoQ_3 (PDF)

■ AUTHOR INFORMATION

Corresponding Authors

Saurabh Das − *Department of Chemistry, Jadavpur University, Kolkata 700032, India;* orcid.org/0000-0002-0455-8760; Phone: +91 9123865911; Email: dasrsv@yahoo.in, saurabh.das@jadavpuruniversity.in; Fax: +91 33 24146223

Asoke Prasun Chattopadhyay − *Department of Chemistry, University of Kalyani, Nadia 741235 West Bengal, India;* orcid.org/0000-0002-2411-1384; Phone: +919836156800; Email: asoke@klyuniv.ac.in; Fax: : +91 33 2582 8282

Partha Sarathi Guin − *Department of Chemistry, Shibpur Dinobundhoo Institution (College), Howrah 711102 West Bengal, India;* orcid.org/0000-0001-9258-9227; Phone: +91 9330083036; Email: parthasg@gmail.com; Fax: +91 33 2688 0344

Authors

Somenath Banerjee − *Department of Chemistry, Shibpur Dinobundhoo Institution (College), Howrah 711102 West Bengal, India; Department of Chemistry, Jadavpur University, Kolkata 700032, India*

Sanjay Roy − *Department of Chemistry, Netaji Subhas Open University, Nadia 741235, India;* orcid.org/0000-0001-6841-4961

Dhanasekaran Dharumadurai − *Department of Microbiology, School of Life Sciences, Bharathidasan University, Tiruchirappalli 620 024, India*

Balaji Perumalsamy − *National Centre for Alternatives to Animal Experiments, Bharathidasan University, Tiruchirappalli 620 024, India*

Ramasamy Thirumurugan − *National Centre for Alternatives to Animal Experiments, Bharathidasan University, Tiruchirappalli 620 024, India*

Complete contact information is available at: https://pubs.acs.org/10.1021/acsomega.1c06125

Notes

The authors declare no competing financial interest.

■ ACKNOWLEDGMENTS

P.S.G. is grateful to UGC, New Delhi, India, for the financial support through the Major Research Project (file no. 41-225/2012(SR) dated 18 July 2012). S.D. gratefully acknowledges support received from UGC-DAE-CSR Collaborative Research Scheme for a project having sanction number UGC-DAE-CSR-KC/CRS/l 9/RC11/0985.

■ ABBREVIATIONS

QH, 1-amino-4-hydroxy-9,10-anthraquinone; CoQ_3, Co(III) complex of 1-amino-4-hydroxy-9,10-anthraquinone; TBAB,

https://doi.org/10.1021/acsomega.1c06125
ACS Omega 2022, 7, 1428−1436

tetrabutyl ammonium bromide; DMSO, dimethyl sulfoxide:; DMF, *N*,*N*-dimethyl formamide

REFERENCES

(1) Hardman, J. -G.; Gilman, A.-G.; Limbird, L.-E. *Goodman and Gilman's The Pharmacological Basis of Therapeutics*, 9th ed.; McGraw-Hill Companies: New York, 1996.

(2) Lim, K. H.; Kim, H. S.; Yang, Y. M.; Lee, S. D.; Kim, W. B.; Yang, J.; Park, J. G. Cellular uptake and antitumor activity of the new anthracycline analog DA-125 in human cancer cell lines. *Cancer Chemother. Pharmacol.* **1997**, *40*, 23−30.

(3) Preobrazhenskaya, M. N.; Tevyashova, A. N.; Olsufyeva, E. N.; Huang, K.-F.; Huang, H.-S. Second generation drugs-derivatives of natural antitumor anthracycline antibiotics daunorubicin, doxorubicin and carminomycin. *J. Med. Sci.* **2006**, *26*, 119−128.

(4) Hu, F. Q.; Liu, L. N.; Du, Y. Z.; Yuan, H. Synthesis and antitumor activity of doxorubicin conjugated stearic acid-g-chitosan oligosaccharide polymeric micelles. *Biomaterials* **2009**, *30*, 6955−6963.

(5) Das, A.; Roy, S.; Mondal, P.; Datta, A.; Mahali, K.; Loganathan, G.; Dharumadurai, D.; Sengupta, P. S.; Akbarsha, M. A.; Guin, P. S. Studies on the interaction of 2-amino-3-hydroxy-anthraquinone with surfactant micelles reveal its nucleation in human MDA-MB-231 breast adinocarcinoma cell. *RSC Adv.* **2016**, *6*, 28200−28212.

(6) Mondal, P.; Roy, S.; Loganathan, G.; Mandal, B.; Dharumadurai, D.; Akbarsha, M. A.; Sengupta, P. S.; Chattopadhyay, S.; Guin, P. S. 1-amino-4-hydroxy-9,10-anthraquinone - An analogue of anthracycline anticancer drugs, interacts with DNA and induces apoptosis in human MDA-MB-231 breast adinocarcinoma cells: Evaluation of structure-activity relationship using computational, spectroscopic and biochemical studies. *Biochem. Biophys. Rep.* **2015**, *4*, 312−323.

(7) Roy, S.; Mondal, P.; Sengupta, P. S.; Dhak, D.; Santra, R. C.; Das, S.; Guin, P. S. Spectroscopic, computational and electrochemical studies on the formation of the copper complex of 1-amino-4-hydroxy-9,10-anthraquinone and effect of it on superoxide formation by NADH dehydrogenase. *Dalton Trans.* **2015**, *44*, 5428−5440.

(8) Roy, S.; Guin, P. S. Solvation of 1-amino-4-Hydroxy-9,10-anthraquinone governs its electrochemical behavior in non-aqueous and aqueous media: A cyclic voltammetry study. *J. Electrochem. Soc.* **2015**, *162*, H124−H131.

(9) Roy, S.; Guin, P. S. Investigation on the interaction of 1-amino-4-hydroxy-9,10 anthraquinone with calf thymus DNA and CTAB micelles. *J. Mol. Liq.* **2015**, *211*, 846−853.

(10) Guin, P. S.; Das, S.; Mandal, P. C. Studies on the formation of a complex of Cu(II) with sodium 1,4-dihydroxy-9,10-anthraquinone-2-sulphonate- An analogue of the core unit of anthracycline anticancer drugs and its interaction with calf thymus DNA. *J. Inorg. Biochem.* **2009**, *103*, 1702−1710.

(11) Guin, P. S.; Mandal, P. C.; Das, S. The binding of a hydroxy-9,10-anthraquinone Cu^{II} complex to calf thymus DNA : Electrochemistry and UV/Vis Spectroscopy. *ChemPlusChem.* **2012**, *77*, 361−369.

(12) Rossi, S.; Tabolacci, C.; Lentini, A.; Provenzano, B.; Carlomosti, F.; Frezzotti, S.; Beninati, S. Anthraquinones danthron and quinizarin exert antiproliferative and antimetastatic activity on murine B16-F10 melanoma cells. *Anticancer Res.* **2010**, *30*, 445−449.

(13) Das, P.; Jain, C. K.; Dey, S. K.; Saha, R.; Chowdhury, A. D.; Roychoudhury, S.; Kumar, S.; Majumder, H. K.; Das, S. Synthesis, crystal structure, DNA interaction and *in vitro* anticancer activity of a Cu(II) complex of purpurin: Dual poison for human DNA topoisomerase I and II. *RSC Adv.* **2014**, *4*, 59344−59357.

(14) Das, P.; Bhattacharya, D.; Karmakar, P.; Das, S. Influence of ionic strength on the interaction of THA and its Cu (II) complex with DNA helps to explain studies on various breast cancer cells. *RSC Adv.* **2015**, *5*, 73099−73111.

(15) Das, P.; Guin, P. S.; Mandal, P. C.; Paul, M.; Paul, S.; Das, S. Cyclic voltammetric studies of 1,2,4-trihydroxy-9,10-anthraquinone, its interaction with calf thymus DNA and anti-leukemic activity on MOLT-4 cell lines: A comparison with anthracycline anticancer drugs. *J. Phys. Org. Chem.* **2011**, *24*, 774−785.

(16) Mandal, B.; Singha, S.; Dey, S. K.; Mazumdar, S.; Mondal, T. K.; Karmakar, P.; Kumar, S.; Das, S. Synthesis, crystal structure from PXRD of a $Mn^{II}(purp)_2$ complex, interaction with DNA at different temperatures and pH and lack of stimulated ROS formation by the complex. *RSC Adv.* **2016**, *6*, 51520−51532.

(17) Nakayama, T.; Okumura, N.; Uno, B. Complementary Effect of Intra- and Intermolecular Hydrogen Bonds on Electron Transfer in *β*-Hydroxy-Anthraquinone Derivatives. *J. Phys. Chem. B.* **2020**, *124*, 848−860.

(18) Tian, W.; Wang, C.; Li, D.; Hou, H. Novel anthraquinone compounds as anticancer agents and their potential mechanism. *Future Med. Chem.* **2020**, 627.

(19) Tikhomirov, A. S.; Shtil, A. A.; Shchekotikhin, A. E. Advances in the Discovery of Anthraquinone-Based Anticancer Agents. *Recent Pat. Anti-Cancer Drug Discovery* **2018**, *13*, 159−183.

(20) Mukherjee Chatterjee, S.; Jain, C. K.; Singha, S.; Das, P.; Roychoudhury, S.; Majumder, H. K.; Das, S. Activity of Co^{II}−quinalizarin: A novel analogue of anthracyclinebased anticancer agents targets human DNA topoisomerase, whereas quinalizarin itself acts via formation of semiquinone on acute lymphoblastic leukemia MOLT-4 and HCT 116 cells. *ACS Omega* **2018**, *3*, 10255−10266.

(21) Błasiak, J.; Gloc, E.; Warszawski, M. A comparison of the *in vitro*genotoxicity of anticancer drugs idarubicin and mitoxantrone. *Acta Biochim. Pol.* **2002**, *49*, 145−155.

(22) Kapuscinski, J.; Daizynkiewicz, Z. Relationship between the pharmacological activity of antitumor drugs ametantrone and mitoxantrone (novatrone) and their ability to condense nucleic acids. *Proc. Natl. Acad. Sci. U. S. A.* **1986**, *83*, 6302−6306.

(23) Ellis, A. L.; Randolph, J. K.; Conway, B. R.; Gewirtz, D. A. Biochemical lesions in DNA associated with the antiproliferative effects of mitoxantrone in the hepatoma cell. *Biochem. Pharmacol.* **2009**, *39*, 1549−1556.

(24) Li, N.; Ma, Y.; Yang, C.; Guo, L.; Yang, X. Interaction of anticancer drug mitoxantrone with DNA analyzed by electrochemical and spectroscopic methods. *Biophys. Chem.* **2005**, *116*, 199−205.

(25) Riahi, S.; Reza Ganjali, M.; Dinarvand, R.; Karamdoust, S.; Bagherzadeh, K.; Norouzi, P. A theoretical study on interactions between mitoxantrone as an anticancer drug and DNA: application in drug design. *Chem. Biol. Drug. Des.* **2008**, *71*, 474−482.

(26) Trachtenberg, B. H.; Landy, D. C.; Franco, V. I.; Henkel, J. M.; Pearson, E. J.; Miller, T. L.; Lipshultz, S. E. Anthracycline-associated cardiotoxicity in survivors of childhood cancer. *Pediatr. Cardiol.* **2011**, *32*, 342−353.

(27) Shi, Y.; Moon, M.; Dawood, S.; McManus, B.; Liu, P. P. Mechanisms and management of doxorubicin cardiotoxicity. *Herz.* **2011**, *36*, 296−305.

(28) Outomuro, D.; Grana, D. R.; Azzato, F.; Milei, J. Adriamycin-induced myocardial toxicity: New solutions for an old problem? *Int. J. Cardiol.* **2007**, *117*, 6−15.

(29) Ferrans, V. J. Overview of cardiac pathology in relation to anthracycline cardiotoxicity. *Cancer Treat. Rep.* **1978**, *62*, 955−961.

(30) Barasch, D.; Zipori, O.; Ringel, I.; Ginsburg, I.; Samuni, A.; Katzhendler, J. Novel anthraquinone derivatives with redox-active functional groups capable of producing free radicals by metabolism: are free radicals essential for cytotoxicity? *Eur. J. Med. Chem.* **1999**, *34*, 597.

(31) Kumbhar, A.; Padhye, S.; Ross, D. Cytotoxic properties of iron-hydroxynaphthoquinone complex in rat hepatocytes. *BioMetals* **1996**, *9*, 235−240.

(32) Bartoszek-Pączkowska, A. Metabolic activation of adriamycin by NADPH cytochrome P450 reductase; overview of its biological and biochemical effects. *Acta Biochim. Pol.* **2002**, *49*, 323−331.

(33) Mandal, B.; Mondal, H. K.; Das, S. In situ reactivity of electrochemically generated semiquinone on emodin and its Cu^{II}/Mn^{II} complexes with pyrimidine based nucleic acid bases and calf thymus DNA: Insight into free radical induced cytotoxicity of anthracyclines. *Biochem. Biophys. Res. Commun.* **2019**, *515*, 505−509.

https://doi.org/10.1021/acsomega.1c06125
ACS Omega 2022, 7, 1428−1436

(34) Das, S.; Saha, A.; Mandal, P. C. Radiation-induced double-strand modification in calf thymus DNA in the presence of 1,2-dihydroxy-9,10-anthraquinone and its Cu(II) complex. *J. Radioanal.Nucl. Chem.* **1996**, *196*, 57−63.
(35) Feng, M.; Yang, Y.; He, P.; Fang, Y. Spectroscopic studies of copper(II) and iron(II) complexes of adriamycin. *Spectrochim. Acta* **2000**, *56*, 581−587.
(36) Wang, H.; Hua, E.; Yang, P. The polarographic and voltammetric behaviour of the copper(II) mitoxantrone complex and its analytical application. *Talanta* **1995**, *42*, 1519−1524.
(37) Yang, P.; Wang, H.; Gao, F.; Yang, B. Antitumor activity of the Cu(II)-mitoxantrone complex and its interaction with deoxyribonucleic acid. *J. Inorg. Biochem.* **1996**, *62*, 137−145.
(38) Pereira, E.; Fiallo, M. M. L.; Garnier-Suillerot, A.; Kiss, T.; Kozłowski, H. Impact of aluminium ions on adriamycin-type ligands. *J. Chem. Soc., Dalton Trans.* **1993**, 455−459.
(39) Italia, T.; Liegro, D. I.; Cestelli, A.; Matzanke, B. F.; Bill, E.; Trautwein, A. X. The interaction of Fe(III), adriamycin and daunomycin with nucleotides and DNA and their effects on cell growth of fibroblasts (NIH-3T3). *BioMetals* **1996**, *9*, 121−130.
(40) Massoud, S. S.; Jordan, R. B. Kinetic and equilibrium studies of the complexation of aqueous iron(III) by daunomycin, quinizarin, and quinizarin-2-sulfonate. *Inorg. Chem.* **1991**, *30*, 4851−4856.
(41) Maroney, M. J.; Day, R. O.; Psyris, T.; Fleury, L. M.; Whitehead, J. P. Structural model for the binding of iron by anthracycline drugs. *Inorg. Chem.* **1989**, *28*, 173−175.
(42) Kolodziejczyk, P.; Garnier-Suillerot, A. Circular dichroism study of the interaction of mitoxantrone, ametantrone and their Pd(II) complexes with deoxyribonucleic acid. *Biochim. Biophys. Acta* **1987**, *926*, 249−257.
(43) Kadarkaraisamy, M.; Mukjerjee, D.; Soh, C. C.; Sykes, A. G. Complexation, crystallography, and electrochemistry of new chelating nicotinyl and thiazolylanthraquinone ligands. *Polyhedron* **2007**, *26*, 4085−4092.
(44) Di Vaira, M.; Orioli, P.; Piccioli, F.; Bruni, B.; Messori, L. Structure of a terbium(III)−quinizarine complex: The first crystallographic model for metalloanthracyclines. *Inorg. Chem.* **2003**, *42*, 3157−3159.
(45) Jabłońska-Trypuć, A.; Świderski, G.; Krętowski, R. K.; Lewandowski, W. Newly Synthesized Doxorubicin Complexes with Selected Metals—Synthesis, Structure and Anti-Breast Cancer Activity. *Molecules* **2017**, *22*, 1106.
(46) Rumyantseva, T. A.; Alekseeva, A. A.; Tkachenko, M. A. Synthesis and Properties of Metal Phthalocyanines Containing Anthraquinone Chromophores. *Rus. J. Gen. Chem.* **2020**, *90*, 1660−1663.
(47) Du, S.; Feng, J.; Lu, X.; Wang, G. The synthesis and characterizations of vanadium complexes with 1,2-dihydroxyanthraquinone and the structure-effect relationship in their in vitro anticancer activities. *Dalton Trans.* **2013**, *42*, 9699−9705.
(48) Yuan, H.; Cheng, B.; Lei, J.; Jiang, L.; Han, Z. Promoting photocatalytic CO_2 reduction with a molecular copper purpurin chromophore. *Nat. Commun.* **2021**, *12*, 1835.
(49) Fain, V. Y.; Zaitsev, B. E.; Ryabov, M. A. Tautomerism of the metal complexes with 1-amino-4-hydroxyanthaquinone. *Russ. J. Coord. Chem.* **2010**, *36*, 396−400.
(50) Bard, A. J.; Faulkner, L. R. *Electrochemical Methods: Fundamentals and Applications*, 2nd ed.; John Wiley & Sons: New York , 1980.
(51) Undre, P. B.; Khirade, P. W.; Rajenimbalkar, V. S.; Helambe, S. N.; Mehrotra, S. C. Dielectric Relaxation in Ethylene Glycol - Dimethyl Sulfoxide Mixtures as a Function of Composition and Temperature. *J. Korean Chem. Soc.* **2012**, *56*, 416−423.
(52) Bose, K.; Kundu, K. Free energies of transfer of some single ions from ethylene glycol to its isodielectric mixtures with acetonitrile at 25°C. *Can. J. Chem.* **1978**, *57*, 2476.
(53) Schäfer, A.; Horn, H.; Ahlrichs, R. Fully Optimized Contracted Gaussian Basis Sets for Atoms Li to Kr. *J. Chem. Phys.* **1992**, *97*, 2571−2577.
(54) Schäfer, A.; Huber, C.; Ahlrichs, R. Fully optimized contracted Gaussian basis sets of triple zeta valence quality for atoms Li to Kr. *J. Chem. Phys.* **1994**, *100*, 5829−5835.
(55) Becke, A. D. Perspective on Density functional thermochemistry. III. The role of exact exchange. *J. Chem. Phys.* **1993**, *98*, 5648−5652.
(56) Becke, A. D. Density-functional exchange-energy approximation with correct asymptotic behavior. *Phys. Rev. A* **1988**, *38*, 3098−3100.
(57) Lee, C.; Yang, W.; Parr, R. G. Development of the Colle-Salvetti correlation-energy formula into a functional of the electron density. *Phys. Rev. B* **1988**, *37*, 785−789.
(58) Orca − an ab initio, DFT and Semi-empirical and SCFMO package, F. Neese, Max Planck Institute for Chemical Energy Conversion, Ruhr, Germany, version 3.0.1.
(59) *Gaussian 09*, Revision A.02, Frisch, M. J. et al., Gaussian, Inc., Wallingford, CT, 2009.
(60) Podolyan, Y.; Leszczynski, J. MaSK: A visualization tool for teaching and research in computational chemistry. *Int. J. Quantum Chem.* **2009**, *109*, 8−16.
(61) Spector, D. L.; Goldman, R. D.; Leinwand, L. A., *Cell: A Laboratory Manual, Culture and Biochemical Analysis of Cells, Cold Spring Harbor Laboratory Press: Cold Spring Harbor*, CSHL Press: New York,1998, pp.341−349.

https://doi.org/10.1021/acsomega.1c06125
ACS Omega 2022, 7, 1428−1436